Analytical–Numerical Modeling of Transient Heat Flux in a Semi-Infinite Medium Using the Duhamel Integral

Anarkhan Kasimakhunova[1], *Qudratbek* Mamarasulov[2*], *Ulugbek* Nigmatov[3], *Li* Xiaohua[4] and *Li* Yun[5]

[1]Fergana State Technical University, Fergana, Uzbekistan
[2]Fergana State Technical University, Fergana, Uzbekistan
[3]Fergana State Technical University, Fergana, Uzbekistan
[4]South China University of Technology, Guangzhou, China
[5]Shenzhen Power Supply Company, Shenzhen, China

Abstract. This article integrates the concepts of general analytical solutions (Model 2) based on the Duhamel integral principle in a semi-infinite body model with digital modelling in the Simulink environment (Model 1) for a thermoelectric battery. The influence of various non-stationary heat loads on the surface temperature of a TEG is analysed. The Duhamel principle allows expressing inhomogeneous boundary conditions of the heat-conduction equation as a superposition of elementary impulses. In Simulink, this integral was implemented numerically through convolution, and the results were compared with analytical solutions. Three classical heat-flux shapes were analysed—polynomially increasing, linearly decreasing, and bell-shaped impulse. A square-pulse heat load was also analysed. The results revealed how the surface temperature's rise–fall behaviour, peak-time delay, and the relationship between heat diffusion and thermoelectric response depend on the heat-flux shape. The numerical and analytical solutions of the Duhamel integral showed good agreement. The differences were mainly attributed to singularity and discrete step selection. This approach is useful for analysing transient thermal processes in thermoelectric batteries and for systems operating with impulsive or pulsating heat sources. The novelty of this study lies in the combined analytical–numerical implementation of the Duhamel integral in the Simulink environment and its application to transient thermoelectric systems under various non-stationary heat-flux profiles.

Keywords: Duhamel principle, thermal diffusion, semi-infinite body, thermoelectric battery, Simulink, transient heat, convolution, heat flux.

1 Introduction

Thermoelectric generators are devices that convert heat flux into electrical energy. Their operation is based on the Seebeck effect, whereby the temperature gradient created by a heat flux causes charge-carrier diffusion inside the material [1, 2]. In thermoelectric modules, the heat flux may not be constant but may vary with time (for example, impulsive or pulsating). Under such conditions, both the temperature difference and the associated Seebeck voltage exhibit transient behaviour [3].

For solving problems of the linear heat equation with inhomogeneous boundary conditions, the Duhamel principle is employed [4]. According to this principle, a time-dependent heat flux can be represented as a sum of independent small impulses. The general solution is obtained by summing the delayed responses of these impulses over time [5, 6]. If q(t) is the time-dependent heat flux (W/m²) applied to the surface of a semi-infinite body, the surface excess temperature is expressed by the following integral:

$$\Delta T(0,t) = \frac{\sqrt{c}}{\chi\sqrt{\pi}}\int_0^t \frac{q(\tau)}{\sqrt{t-\tau}}\,\mathrm{d}\tau, t > 0 \quad (1)$$

In this context, χ denotes the thermal conductivity (W/(m·K)), and c represents the thermal diffusivity (m²/s). The kernel $1/\sqrt{t-\tau}$ in the integral expresses the decay of the influence of a given impulse over time due to thermal diffusion; here, τ is the moment at which the impulse is applied, and t is the observation time [7]. If q(t) is a constant heat flux q_0 (for example, for $t_0 \leq t \leq t_1$), integral (1) can be evaluated analytically, yielding a square-root-type expression for the surface temperature:

$$\Delta T \propto \sqrt{t-t_0} - \sqrt{t-t_1} \quad (2)$$

When modelling heat flux in a thermoelectric battery, the thickness of the battery element can be considered infinite within the time interval during which heat is applied [8, 9]. This simplification implies that heat transfer occurs only in one direction (perpendicular to the surface). According to Fourier's law, the heat flux is related to the temperature gradient inside the material [10–12]:

$$q = -\chi\frac{\partial T}{\partial x} \quad (3)$$

The Duhamel principle is based on the superposition property of linear systems. The general solution is obtained by summing the delayed responses of these impulses over time. [13]. In integral (1), the kernel $1/\sqrt{t-\tau}$ reflects the attenuation of an impulse's effect during the thermal diffusion process: as t−τ increases, the contribution of the impulse to the surface temperature diminishes. In cases where the heat flux is continuous, the Duhamel integral determines the temperature evolution while accounting for the inertial properties of the solid medium (i.e., its heat capacity and thermal diffusivity) [14, 15].

However, existing studies mainly focus on either analytical or numerical approaches separately. The combined implementation of the Duhamel integral within the Simulink environment for thermoelectric applications

*Corresponding author: mamarasulovqudratillo7@gmail.com

under transient heat flux conditions remains insufficiently explored. This study aims to fill this gap.

2 Materials and Methods

In the Model 1 simulation, numerical evaluation of integral (1) was performed using the Simulink environment (MATLAB). The time-dependent heat flux q(t) was generated in a Signal Builder block (e.g., a square pulse applied from 2 s to 4 s). Two computational approaches were employed to evaluate the Duhamel integral for a semi-infinite body:

1. Duhamel_stream – a streaming algorithm implemented inside a MATLAB Function block. For each input sample q(n), the algorithm computes the temperature rise by convolving it with the kernel $w[k] = T_s/\sqrt{(k-1/2)T_s}$, where T_s is the sampling time. To smooth the singularity, the first kernel element was set to zero. The accuracy of the result depends on the number of samples (window size) and the time step. The output dT was sent to a Scope block and stored in the object out.T_stream.
2. Duhamel_theor – a theoretical solution computed in a MATLAB Function block in accordance with the analytical expression (1). This block takes the time variable t as input and evaluates the surface temperature using the formula for a constant heat flux q_0 applied over the interval 2–4 s:

$$\Delta T(0,t) = \frac{2q_0\sqrt{c}}{\chi\sqrt{\pi}}\left(\sqrt{t-2} - H(t-4)\sqrt{t-4}\right) \tag{4}$$

where H(·) denotes the Heaviside function.

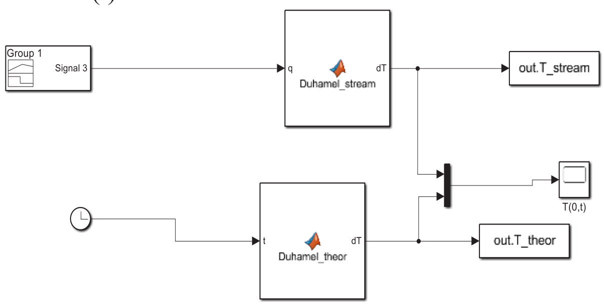

Fig. 1. Duhamel-integral computation model for a semi-infinite body (Model 1)

The overall block diagram of the simulation model is presented in Fig. 1. Here, the output q from the Signal Builder block is fed into the Duhamel_stream block; the resulting dT signal is monitored using a Scope block and saved to the MATLAB workspace via To Workspace blocks under the names out.T_stream and out.T_theor.

In Model 2, three classical time-dependent heat-flux profiles—polynomial growth, linear decay, and a bell-shaped impulse—were simulated by implementing the Duhamel integral within the Simulink platform. The general structure is shown in Fig. 2. Three subsystem blocks generate alternative surface heat-flux profiles: the polynomial generator outputs $q_0 t^n$; the linearly decaying generator outputs $q_0(1-t/t_0)$ within the interval $q_0(1-t/t_0)$; the bell-shaped generator produces $4q_0[t/t_0-(t/t_0)^2]$ over the same interval. Manually controlled switches ensure that only one signal at a time is routed to the Duhamel block. The Clock block provides the current simulation time, while Constant blocks define the values of χ, c, and the heat-flux amplitude q_0 . The signals are then passed to a dedicated MATLAB Function block, duhamel_q2T, where discrete convolution is performed.

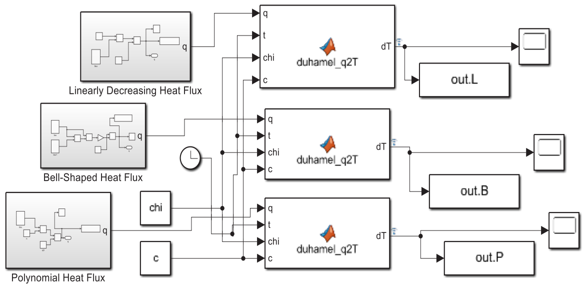

Fig. 2. Model of three classical time-dependent heat-flux profiles (Model 2)

In the MATLAB Function block, memory arrays are preallocated to their maximum length and indexed using a continuous counter. At each time step, the current sample is appended, after which the accumulated waveform is processed using the analytical expression for the kernel integral

$$\int_{t_{i-1}}^{t_i} \mathrm{d}\tau/\sqrt{t_k-\tau} = 2\left(\sqrt{t_k-t_{i-1}} - \sqrt{t_k-t_i}\right) \tag{5}$$

to compute the summation. The resulting value is multiplied by the global factor $\sqrt{c}/(\chi\sqrt{\pi})$. The discrete time step was set to $T_s = 10^{-3}$, and the simulation time was chosen as t_0 or $2t_0$, depending on the heat-flux profile.

Three classical dynamic heat-flux shapes were considered:

1. Polynomial growth: $q(t) = q_0\, t^n$. with $n = 0.5$, i.e., $q \propto \sqrt{t}$ Such a signal models a gradually increasing energy source (e.g., a laser ramping up to full power).
2. Linear decay: $q(t) = q_0(1-t/t_0)$, $0 \le t \le t_0$ and zero afterward. This represents a simplified model of a uniformly weakening heat source.
3. Bell-shaped impulse: $q(t) = 4q_0[t/t_0 - (t/t_0)^2]$, $0 \le t \le t_0$ and zero afterward. The signal starts at zero, reaches its maximum at $t_0/2$, and returns to zero at t_0 , representing a symmetric impulse with finite rise and fall times.

All signals were windowed using a saturation block $\tau = \max(0, \min(t/t_0, 1))$, ensuring that they remain active only within $0 \le t \le t_0$ and vanish outside this interval. This prevents physically meaningless negative heat-flux values.

3 Results

In the numerical modelling (Model 1), the accuracy of the results depends on the time-step size (e.g., $T_s = 5 \times 10^{-4}$) and window length (e.g., 4000 samples). The Scope output for a square heat pulse applied from 2 s to 4 s is shown in Fig. 3. The yellow curve represents the Duhamel_stream result, while the blue curve corresponds to the Duhamel_theor (analytical) solution. The surface temperature begins at zero at t = 2 s and increases according to the square-root law, which confirms the

 https://doi.org/10.1051/e3sconf/202672902002

theoretical prediction of the Duhamel integral solution.

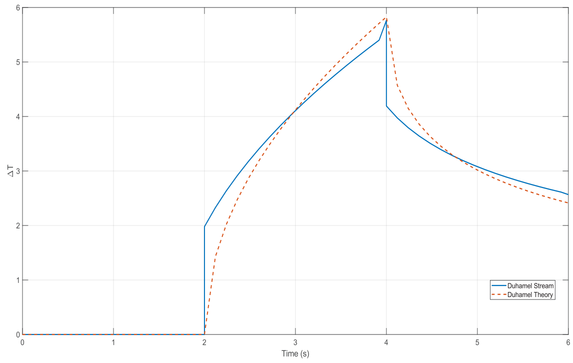

Fig. 3. Duhamel-equation plot for a square heat pulse (Model 1)

After the simulation results were saved using the To Workspace block, both signals were plotted together in MATLAB, and the difference between them was analysed (Fig. 4). In Fig. 4(a), the numerical (Duhamel_stream) and analytical (Duhamel_theor) solutions are compared, together with their difference. Fig. 4(b) shows the corresponding error signal separately. Throughout the main duration of the pulse (2–4 s), no significant deviation is observed between the two curves. The discrepancies appear mainly at the pulse boundaries (t = 2 s and t = 4 s), which is attributed to the singular nature of the kernel and limitations of discrete time-step approximation. This behaviour arises because the singular kernel $1/\sqrt{t-\tau}$ in the Duhamel integral cannot be fully captured with a discrete time step, and the abrupt transitions of the applied flux introduce slight fluctuations (spikes) in the numerical integration. In the intermediate region, however, both curves match perfectly.

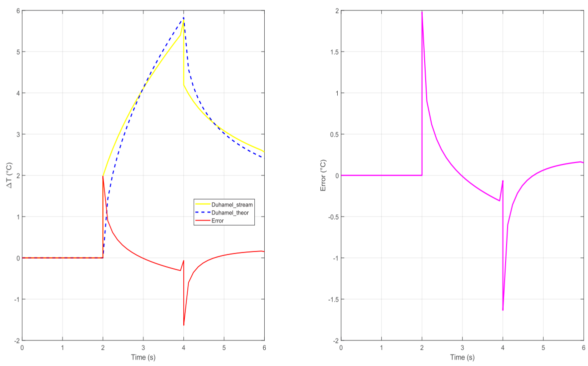

Fig. 4. (a) Comparison of numerical (Duhamel_stream) and analytical (Duhamel_theor) solutions; (b) corresponding error signal between the two methods.

From the numerical comparison, the accuracy indicators were determined as follows: the RMS error is 0.423488 °C, and the maximum error is 1.978757 °C. This discrepancy arises at points where the heat flux undergoes abrupt changes; however, such ideal step transitions do not occur in real thermoelectric batteries due to thermal inertia. Increasing the window length and reducing the time step in the discrete integral further decreases the numerical error.

To validate the numerical model (Model 2), analytical solutions were derived for each type of heat-flux profile. For example, in the polynomial case with $n = 1/2$,

$$\Delta T(0,t) = \frac{\sqrt{\pi}}{2}\frac{\sqrt{c}}{\chi} q_0 \, t, \tag{6}$$

meaning that the temperature increases linearly with time. For the linearly decaying and bell-shaped impulses, the integral is evaluated piecewise, and the resulting temperature responses exhibit characteristic peaks.

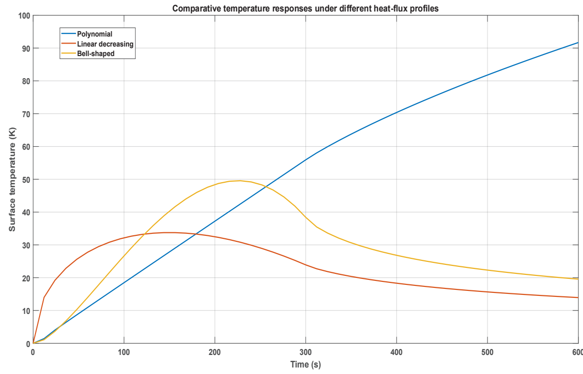

Fig. 5. Comparative surface-temperature responses under different transient heat-flux profiles obtained using the Duhamel-integral model.

For comparative analysis, the temperature responses corresponding to the polynomial, linearly decreasing, and bell-shaped heat-flux profiles were plotted on the same axis, as shown in Fig. 5.

3.1 Polynomial Heat Flux (n=0.5)

Fig. 6 illustrates the Simulink implementation of the polynomial heat-flux model. The subsystem generates a gradually increasing heat-flux signal according to the power-law dependence $q \propto t^{0.5}$ and evaluates the corresponding surface-temperature response using the Duhamel-integral block. According to theory, convolution with the kernel $1/\sqrt{t-\tau}$ increases the exponent by one, implying that the surface temperature should grow linearly. The comparative temperature response corresponding to the polynomial heat-flux profile is presented in Fig. 5. Fig. 5 shows the computed temperature response for $t_0 = 300\,s$. After the initial filling of the memory buffer, the curve becomes almost perfectly linear, confirming the analytical expression $\Delta T = (\sqrt{\pi}/2)(\sqrt{c}/\chi)q_0\,t$. The slight curvature near t≈0 results from discrete time-step errors. Overall, the simulation confirms that $\Delta T \propto t$.

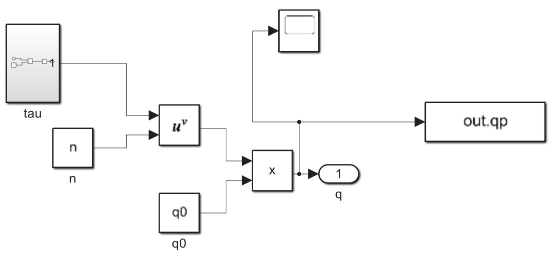

Fig. 6. Simulink implementation of the polynomial heat-flux model.

3.2 Linearly Decreasing Heat Flux

Fig. 7 presents the Simulink implementation of the linearly decreasing heat-flux model. In this subsystem, the heat flux decreases linearly with time and is supplied to the duhamel_q2T block for numerical convolution and transient temperature evaluation. The signal $q(t) = q_0(1 - t/t_0)$ starts at q_0 within the interval $[0, t_0]$ and decreases linearly to zero by $t=t_0$. When this triangular profile is convolved with the kernel, the surface temperature first increases, then reaches a maximum as a result of the balance between the declining heat-source strength and the continuing effect of thermal diffusion. The corresponding comparative temperature response for the linearly decreasing heat-flux profile is shown in Fig. 5. Theoretical analysis predicts that the maximum occurs near $t_0/2$. Fig. 5 presents the result for t_0=300 s: the temperature rises to approximately 32 K, and the peak occurs at around 150 s, which is fully consistent with the theoretical prediction. Although the heat flux becomes zero after , the surface temperature decreases only gradually, because the energy accumulated within the medium continues to diffuse outward. The tail decays approximately as $t^{-1/2}$ (for $t_0 = 300$). The peak indeed appears near $t_0/2 \approx 150$.

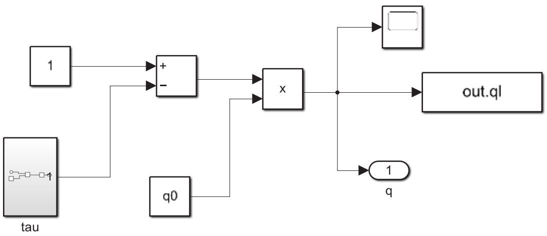

Fig. 7. Simulink implementation of the linearly decreasing heat-flux model.

3.3 Bell-Shaped Heat Flux

Fig. 8 shows the Simulink implementation of the bell-shaped heat-flux model. The subsystem generates a symmetric transient heat-flux pulse, while the Duhamel-integral computation block determines the delayed surface-temperature response caused by thermal diffusion inertia. The bell-shaped signal $q(t) = 4q_0[t/t_0 - (t/t_0)^2]$ takes the value zero at t=0, reaches its maximum at $t_0/2$, and returns to zero at $t = t_0$. Even after the flux begins to decrease, heat continues to arrive at the boundary for a certain period, causing the surface temperature to continue increasing for some time. Both theoretical analysis and numerical simulations show that the maximum surface temperature occurs at approximately $3t_0/4$. Fig. 5 presents the result for $t_0 = 300$: the temperature reaches about 47 K, and the peak appears at roughly 225 s (i.e., $0.75t_0$). Beyond this point, diffusion becomes dominant and the temperature decreases gradually. Although the heat-flux peak occurs at $t_0/2$, the delayed peak of the surface temperature is explained by thermal diffusion inertia (for $t_0 = 300$). Thus, the maximum is observed near $3t_0/4$.

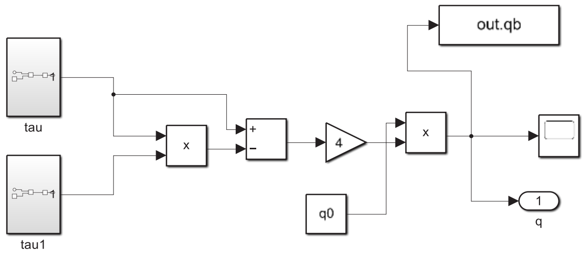

Fig. 8. Simulink implementation of the bell-shaped heat-flux model.

4 Discussion

The physical interpretation of the Duhamel integral is that the contribution of each heat impulse applied to the surface decays over time according to the law $1/\sqrt{t - \tau}$ during the diffusion process. For a square heat pulse, the surface temperature initially rises rapidly from zero, and as the heat flux continues, the growth rate slows due to energy absorption into the medium. After the flux is removed, the temperature begins to decrease gradually due to diffusion. In the semi-infinite model, since the depth of the medium is unbounded, the temperature does not eventually return to zero but continues to grow as t ; in real thermoelectric batteries, however, the presence of finite boundaries leads to long-term thermal stabilization.

In thermoelectric modules, when the heat flux varies in time, the temperature difference also changes inertially, leading to a delayed formation of the Seebeck voltage. This delay is determined by the thermal diffusivity c and thermal conductivity χ. Under a square heat pulse:

- the electromotive force (EMF) rises rapidly at the beginning,
- during the pulse, heat continues to propagate inward and the EMF approaches a saturation-like value,
- after the flux stops, the EMF decreases slowly.

These results are useful for analysing transient thermoelectric processes, particularly in systems with pulsating heat sources (e.g., TEGs integrated with solar panels). Moreover, the simulations successfully reproduced the analytical behaviour of the Duhamel integral for the three dynamic heat-flux profiles. The following physical insights emerge:

- Energy accumulation and diffusion: The kernel $1/\sqrt{t - \tau}$ assigns greater weight to more recent heat input. In the polynomial case, while the flux is increasing, the most recent values dominate, leading to a monotonic increase in ΔT. When the flux begins to decrease, previously deposited heat continues to diffuse, causing the peak to occur later.
- Peak times: For a linearly decreasing flux, the competition between source decay and diffusive retention produces a maximum at $t_0/2$; for a bell-shaped flux, the asymmetric contributions of the rising and falling halves shift the peak to $3t_0/4$. Determining such peak times can be valuable for evaluating thermal inertia in heat-battery testing.
- Units and scaling: SI units were used throughout the modelling: q in W/m², χ in W/(m·K), and c in m²/s.

The prefactor $\sqrt{c}/(\chi\sqrt{\pi})$ demonstrates that the temperature response increases when diffusivity c is higher or thermal conductivity χ is lower. This highlights the role of material properties: materials with high conductivity and low diffusivity (e.g., copper) experience smaller temperature rises for the same heat flux.

The post-peak decay of the curve also provides insight. Because a semi-infinite medium continues absorbing heat, the surface temperature decreases slowly, approximately as $t^{-1/2}$. In real finite plates or multilayer systems, once the thermal wave reaches the backside, the decay rate becomes faster.

5 Conclusion

The combination of analytical solutions based on the Duhamel principle and numerical modelling in Simulink enabled a comprehensive analysis of the effects of various time-dependent heat-flux profiles on the surface temperature of a semi-infinite body. Under polynomially increasing flux, the surface temperature grows linearly; in contrast, linearly decreasing and bell-shaped pulses exhibit distinct peak times consistent with theoretical predictions. The simulation results showed good agreement with theoretical analysis and clearly demonstrated the sensitivity of the method to kernel singularity, discrete time-step size, and material parameters. The findings indicate that in designing TEGs exposed to unconventional (transient) heat loads, the processes of heat diffusion and energy accumulation must be carefully considered. Furthermore, this method provides a basis for evaluating system responses in TEG designs that incorporate external cooling conditions and material-property variations. In future research, this approach can be applied to the optimization of TEG generators operating with impulsive heat sources and to the analysis of multilayer thermal-transfer systems.

Anarkhan Kasimakhunova – conceptualization, supervision, and scientific guidance.
Qudratbek Mamarasulov – numerical modelling, Simulink implementation, data analysis, and manuscript preparation.
Ulugbek Nigmatov – methodology development and analytical analysis.

The data used to support the findings of this study are included within the article.
Additional simulation data and modelling files can be provided by the corresponding author upon reasonable request.

References

1. V.D. Beybalaev, A.A. Aliverdiev, J. Hristov, Transient heat conduction in a semi-infinite domain with a memory effect: Analytical solutions with a Robin boundary condition, Fractal Fract. **7**, 770 (2023). https://doi.org/10.3390/fractalfract7100770
2. S. Dalola, M. Ferrari, V. Ferrari, M. Guizzetti, D. Marioli, A. Taroni, Characterization of thermoelectric modules for powering autonomous sensors, IEEE Trans. Instrum. Meas. **58**, 99–107 (2009). https://doi.org/10.1109/TIM.2008.928405
3. L. Hou, S. Tan, L. Yang, Z. Zhang, N.W. Bergmann, Autonomous wireless sensor node with thermal energy harvesting for temperature monitoring of industrial devices, Int. J. Online Eng. **13**, 75–81 (2017). https://doi.org/10.3991/ijoe.v13i04.6802
4. O. Hogblom, R. Andersson, Analysis of thermoelectric generator performance by use of simulations and experiments, J. Electron. Mater. **43**, 2246–2254 (2014). https://doi.org/10.1007/s11664-014-3020-x
5. J. Hristov, Semi-derivative integral method to transient heat conduction in a semi-infinite medium with time-dependent (power-law) boundary conditions, Therm. Sci. **25**, 3557–3568 (2021). https://doi.org/10.2298/TSCI201014143H
6. J. Hristov, The Duhamel Method in Transient Heat Conduction: A Rendezvous of Classics and Modern Fractional Calculus (Bentham Science Publishers, 2022). https://doi.org/10.2174/97898150519331220300007
7. M.O. Atazhonov, Q. Mamarasulov, L.M. Gimaeva, R.I. Suleimanov, Mathematical model of a photoelectric thermal electric energy converter under load, Proc. SPIE **13662**, 136620O (2025). https://doi.org/10.1117/12.3072651
8. S. Kato, S. Matsuda, A new analytical method for solving the problem of one-dimensional transient heat conduction in a slab by using the temperature solutions of semi-infinite solids, Mech. Eng. J. **4**, 17-00096 (2017). https://doi.org/10.1299/mej.17-00096
9. S. Lineykin, S. Ben-Yaakov, Analysis of thermoelectric coolers by a SPICE-compatible equivalent-circuit model, IEEE Power Electron. Lett. **3**, 63–66 (2005). https://doi.org/10.1109/LPEL.2004.840832
10. D. Milić, A. Prijić, L. Vračar, Z. Prijić, Characterization of commercial thermoelectric modules for application in energy harvesting wireless sensor nodes, Appl. Therm. Eng. **121**, 74–82 (2017). https://doi.org/10.1016/j.applthermaleng.2017.03.029
11. Y. Moumouni, R.J. Baker, Improved SPICE modeling and analysis of a thermoelectric module, Proc. IEEE MWSCAS, 1–4 (2015). https://doi.org/10.1109/MWSCAS.2015.7282015
12. S.B. Riffat, X. Ma, Thermoelectrics: A review of present and potential applications, Appl. Therm. Eng. **23**, 913–935 (2003). https://doi.org/10.1016/S1359-4311(03)00012-7
13. A. Kasimakhunova, Q. Mamarasulov, Modeling of the dynamics of charge carriers of a photocell under non-stationary lighting conditions in the Simulink environment, EPJ Web Conf. **356**, 02001 (2026). https://doi.org/10.1051/epjconf/202635602001
14. P. Singh, Errors incurred in local convective heat transfer coefficients obtained through transient one-dimensional semi-infinite conduction modeling: A computational heat transfer study, Energies **15**, 7001 (2022). https://doi.org/10.3390/en15197001
15. A.S. Saidov, Sh.N. Usmonov, M.U. Kalanov, Kh.M. Madaminov, D.A. Nishanova, Effect of Gamma Irradiation on Photoconductivity and Photosensitivity of Si1-xSnx Solid Solutions, Appl. Sol. Energy **47**, 48–51 (2011). https://doi.org/10.3103/S0003701X11010142